

Valence-differential spectroscopy of Co–Fe cyanide films

Y. Moritomo,^{a)} F. Nakada, and Y. Kurihara

Department of Physics, University of Tsukuba, Tsukuba 305-8577, Japan

(Received 13 January 2009; accepted 3 March 2009; published online 20 March 2009)

Electrochromism is extensively investigated for practical application of display and memory devices. To develop the material, reliable information on the optical and electronic properties of the solid film is indispensable. Here, we propose valence-differential spectroscopy that can selectively extract the spectral components related to the oxidized/reduced metal site. We applied the spectroscopy to $\text{Co}^{2+}\text{--Fe}^{2+\delta}$ and $\text{Co}^{2+\delta}\text{--Fe}^{2+}$ cyanide films with finely control of averaged valence (δ) of the transition metal by external electric pulses. The spectroscopy revealed transition energy E , width Γ , and oscillator strength f of the spectral components related to the transition metal. © 2009 American Institute of Physics. [DOI: 10.1063/1.3103561]

Electrochromism, especially in films of transition metal complex, is attracting current interest of material scientists because the electronic structure (color of the film) can be widely tuned by substitution of the transition metal. For example, chemical substitution of Prussian blue analog, $\text{Na}_x\text{M}[\text{Fe}(\text{CN})_6]_y\cdot z\text{H}_2\text{O}$ (M is a transition metal) changes the color from red ($M=\text{Co}$), blue ($M=\text{Fe}$), and yellow ($M=\text{Ni}$). Recently, Gotoh *et al.*¹ reported a simple synthesis procedure of Prussian blue nanoparticle inks, which is a breakthrough toward a practical display device.² The Prussian blue analog consists of a cyanobridged rock-salt-type network, $\text{--NC--Fe--CN--M--NC--Fe--CN--}$, and guest species, Na^+ ions and H_2O molecules, accommodated in the nanopores of the network.³ The electrochromism in this system is ascribed to oxidation/reduction of the transition metal site and subsequent outgoings/incomings of the Na^+ ions.^{4,5} In spite of the promising functionality, there exists few quantitative reports on the optical properties of the Prussian blue analog⁶ and assignment of the optical transitions is still controversial, especially in the higher energy region. So far, Nakada *et al.*⁷ and Igarashi *et al.*⁸ synthesized a series of valence-controlled Co–Fe films ($\text{Na}_{0.84-\delta}\text{Co}[\text{Fe}(\text{CN})_6]_{0.71}\cdot 3.8\text{H}_2\text{O}$ and $\text{Na}_{1.60-\delta}\text{Co}\times[\text{Fe}(\text{CN})_6]_{0.90}\cdot 2.9\text{H}_2\text{O}$) and investigated δ -dependence of absorption spectra. Based on the δ -dependence, they decomposed the absorption spectra and assigned the respective spectral components. However, the decomposition of rather broad spectra has ambiguities and is model dependent. Here, we propose a more accurate and unambiguous spectroscopy, i.e., valence-differential spectroscopy, that can extract the spectral components related to the oxidized/reduced metal site.

We synthesized valence-controlled Co–Fe films, $\text{Na}_{0.84-\delta}\text{Co}[\text{Fe}(\text{CN})_6]_{0.71}\cdot 3.8\text{H}_2\text{O}$ ($\delta=0.14$; 960 nm in thickness) and $\text{Na}_{1.60-\delta}\text{Co}\times[\text{Fe}(\text{CN})_6]_{0.90}\cdot 2.9\text{H}_2\text{O}$ ($\delta=0.16$; 650 nm in thickness) on an indium tin oxide (ITO) transparent electrode by an electrochemical method. Chemical compositions of the prepared films were determined by inductively coupled plasma and standard microanalytical methods. These compounds belong to the face-centered cubic ($Fm\bar{3}m$; $Z=4$) with lattice constant of 1.03 nm. Details of the synthesis and

characterization were described elsewhere.^{7,8} In these films, magnitude of δ can be controlled by oxidation process of nondoped film ($\delta=0$). Electronic configuration of the nondoped film is high-spin Co^{2+} ($t_{2g}^5e_g^2$) and low-spin Fe^{2+} (t_{2g}^6). We confirmed a linear relation between δ and total current q during the oxidization process. Infrared absorption spectra revealed that the oxidization site is Fe (Co) for the former (latter) systems (*vide infra*); extended chemical formulas are $\text{Na}_{0.84-\delta}\text{Co}[\text{Fe}^{2+}(\text{CN})_6]_{0.71-\delta}[\text{Fe}^{3+}(\text{CN})_6]_{\delta}\cdot 3.8\text{H}_2\text{O}$ and $\text{Na}_{1.60-\delta}\text{Co}_{1-\delta}\text{Co}_{\delta}^{3+}[\text{Fe}(\text{CN})_6]_{0.90}\cdot 2.9\text{H}_2\text{O}$. For convenient of explanation, we will call the films as $\text{Co}^{2+}\text{--Fe}^{2+\delta}$ and $\text{Co}^{2+\delta}\text{--Fe}^{2+}$.

We schematically show in Fig. 1(a) the valence-differential spectroscopy. We sandwiched an aqueous solution containing 1 mol/l NaCl between Prussian blue analog films grown on ITO transparent electrode. Central part of the right-side film, which works as a counter electrode, was removed. Magnitude of δ was finely controlled by electric pulses, and was estimated from the induced total current q . Figure 1(b) shows relative change ($\Delta\delta$) in the averaged valence in $\text{Na}_{0.84-\delta}\text{Co}[\text{Fe}(\text{CN})_6]_{0.71}\cdot 3.8\text{H}_2\text{O}$ ($\delta=0.14$) film against the number of the electric pulse, 0.25 V in height and 1 s in duration. Magnitude of δ increases in a rate of 0.012 electrons/Co pulse. Reversely, δ can be reduced by negative electronic pulses (see inset of Fig. 2). Thus, we can finely and reversibly control the δ value by an external electric pulse. Absorption spectra $\alpha(h\nu)$ in the visible-violet region (1–4 eV) were measured with a conventional monochromator system with a xenon lamp. The transmitted light was

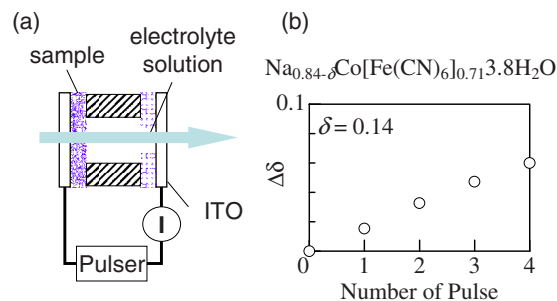


FIG. 1. (Color online) (a) Schematic illustration of valence-differential spectroscopy. (b) Relative change ($\Delta\delta$) in the averaged valence against the number of the electric pulses, 0.25 V in height and 1 s in duration, in $\text{Na}_{0.84-\delta}\text{Co}[\text{Fe}(\text{CN})_6]_{0.71}\cdot 3.8\text{H}_2\text{O}$ ($\delta=0.14$) film.

^{a)}Electronic mail: moritomo@sakura.cc.tsukuba.ac.jp.

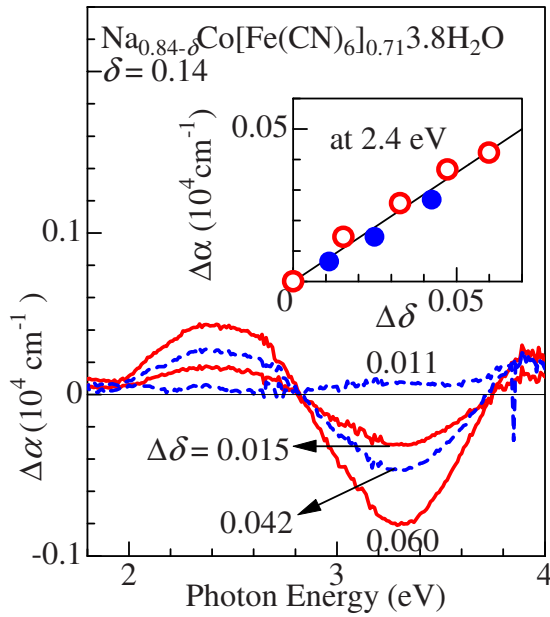


FIG. 2. (Color online) Valence-differential absorption spectra $\Delta\alpha(h\nu)$ against relative change $\Delta\delta$ in the averaged valence in $\text{Na}_{0.84-\delta}\text{Co}[\text{Fe}(\text{CN})_6]_{0.71}\cdot 3.8\text{H}_2\text{O}$ ($\delta=0.14$) film at 300 K. Solid (broken) curves were measured in the $\Delta\delta$ -increasing (-decreasing) run. Inset shows relative change ($\Delta\alpha$) in absorption coefficient at 2.4 eV against $\Delta\delta$. Open (closed) circles were obtained in the Δ -increasing (-decreasing) run. Straight line is a result of least-square fitting.

focused on a Si-photodiode, and a lock-in detection was adopted to enhance the S/N ratio. $\alpha(h\nu)$ spectra in the infrared region were measured with a Fourier-transform-type spectrometer. We emphasize that the small sample size (2 mm in thickness and 2 cm² in area) enables our method to combine other microspectroscopic technique. This is an advantage point compared to an *in situ* electrochemical optical measurement.

Figure 2 shows valence-differential absorption spectra $\Delta\alpha(h\nu)$ against $\Delta\delta$ in $\text{Co}^{2+}\text{-Fe}^{2+\delta}$ at 300 K. Solid curves were measured in the $\Delta\delta$ -increasing run (oxidization process), while broken curves were measured in the $\Delta\delta$ -decreasing run (reduction process). The oxidization process of the Fe site increases (decreases) the density of the Fe^{3+} (Fe^{2+}) state. Then, the positive (negative) spectral component at $\Delta\delta=0.015$ and 0.060 can be assigned to the optical transitions related to the Fe^{3+} (Fe^{2+}) state. Reversely, the reduction process of the Fe site decreases (increases) the density of the Fe^{3+} (Fe^{2+}) state, and suppresses $\Delta\alpha(h\nu)$ spectra magnitude of $\Delta\alpha$ at 2.4 eV and increases linearly with $\Delta\delta$, as shown in the inset.

Figure 3(a) shows $\alpha(h\nu)$ and $\Delta\alpha(h\nu)$ spectra around the CN stretching mode of $\text{Co}^{2+}\text{-Fe}^{2+\delta}$. The $\Delta\alpha(h\nu)$ spectrum shows positive (negative) change in the CN stretching mode within $[\text{Fe}^{3+}(\text{CN})_6]^{3-}$ ($[\text{Fe}^{2+}(\text{CN})_6]^{4-}$),^{7,9} indicating the hole doping on the Fe site. Figure 3(b) shows $\alpha(h\nu)$ and $\Delta\alpha(h\nu)$ spectra of $\text{Co}^{2+\delta}\text{-Fe}^{2+}$. The $\Delta\alpha(h\nu)$ spectrum shows a derivative profile, indicating a rigid blueshift⁸ of the CN stretching mode within $[\text{Fe}^{2+}(\text{CN})_6]^{4-}$. This indicates that the holes are introduced on the Co site. The rigid shift may be ascribed to the doping-induced volume change.⁸

Figure 3(c) shows $\alpha(h\nu)$ and $\Delta\alpha(h\nu)$ spectra of $\text{Co}^{2+}\text{-Fe}^{2+\delta}$ at 300 K, respectively. In the $\alpha(h\nu)$ spectrum, three broad structures are observed at 2.4, 3.2, and 3.8 eV.

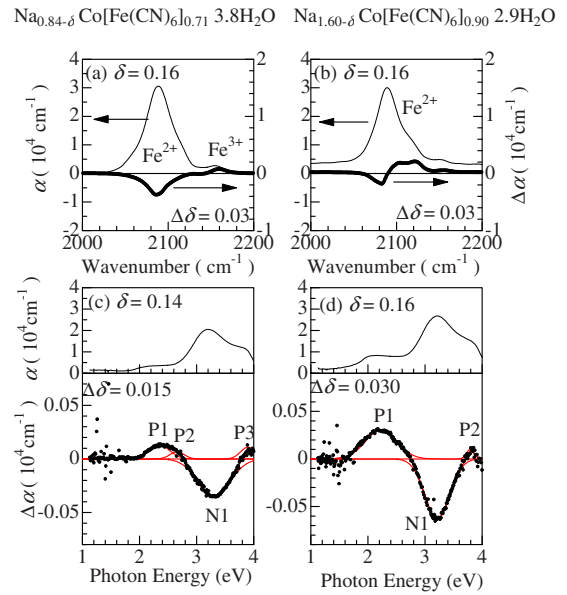


FIG. 3. (Color online) (a) Absorption spectrum $\alpha(h\nu)$ and valence-differential absorption spectrum $\Delta\alpha(h\nu)$ of $\text{Na}_{0.84-\delta}\text{Co}[\text{Fe}(\text{CN})_6]_{0.71}\cdot 3.8\text{H}_2\text{O}$ ($\delta=0.14$) film at 300 K around the CN stretching mode. The absorption band indicated by Fe^{3+} (Fe^{2+}) is due to the CN stretching mode within $[\text{Fe}^{3+}(\text{CN})_6]^{3-}$ ($[\text{Fe}^{2+}(\text{CN})_6]^{4-}$). (b) $\alpha(h\nu)$ and $\Delta\alpha(h\nu)$ spectra of $\text{Na}_{1.60-\delta}\text{Co}[\text{Fe}(\text{CN})_6]_{0.90}\cdot 2.9\text{H}_2\text{O}$ ($\delta=0.16$) film at 300 K around the CN stretching mode. (c) $\alpha(h\nu)$ and $\Delta\alpha(h\nu)$ spectra of $\text{Na}_{0.84-\delta}\text{Co}[\text{Fe}(\text{CN})_6]_{0.71}\cdot 3.8\text{H}_2\text{O}$ ($\delta=0.16$) film at 300 K. (d) $\alpha(h\nu)$ and $\Delta\alpha(h\nu)$ spectra of $\text{Na}_{1.60-\delta}\text{Co}[\text{Fe}(\text{CN})_6]_{0.90}\cdot 2.9\text{H}_2\text{O}$ ($\delta=0.16$) film at 300 K. Solid curves in the lower panel of (c) and (d) represent decomposition of the $\Delta\alpha(h\nu)$ spectrum with four Gaussian functions.

The $\Delta\alpha(h\nu)$ spectrum clearly indicates positive, negative, and positive signals around the respective structures. We further found a shoulder structure at 2.7 eV in the $\Delta\alpha(h\nu)$ spectrum, suggesting an extra component. We decompose the spectrum with four Gaussian functions, i.e., $P1$, $P2$, $N1$, and $P3$. Solid curves in the lower panel in Fig. 3(c) are results of the least-square fitting. The shoulder structure at 2.7 eV is satisfactorily reproduced by the four-component fitting. Figure 3(d) shows $\alpha(h\nu)$ and $\Delta\alpha(h\nu)$ spectra of $\text{Co}^{2+\delta}\text{-Fe}^{2+}$ at 300 K, respectively. The $\Delta\alpha(h\nu)$ spectrum shows positive, negative, and positive signals at 2.2, 3.2, and 3.8 eV. So, we decompose the spectrum with four Gaussian functions, i.e., $P1$, $N1$, and $P2$ [see solid curves in the lower panel of Fig. 3(d)]. Thus obtained optical constants, transition energy E , width Γ , and oscillator strength f , of the respective components are listed in Table I together with the assignments

TABLE I. Transition energy E , width Γ , and oscillator strength f of $\text{Na}_{0.84-\delta}\text{Co}[\text{Fe}(\text{CN})_6]_{0.71}\cdot 3.8\text{H}_2\text{O}$ ($\delta=0.14$: $\text{Co}^{2+}\text{-Fe}^{2+\delta}$) film and $\text{Na}_{1.60-\delta}\text{Co}[\text{Fe}(\text{CN})_6]_{0.90}\cdot 2.9\text{H}_2\text{O}$ ($\delta=0.16$: $\text{Co}^{2+\delta}\text{-Fe}^{2+}$) film.

Compound	Component	E (eV)	Γ (eV)	f	Assignments
$\text{Co}^{2+}\text{-Fe}^{2+\delta}$	$P1$	2.34	0.43	0.010/Fe	$\text{Co}^{2+} \rightarrow \text{Fe}^{3+}$
	$P2$	2.65	0.29	0.004/Fe	$\text{CN}^- \rightarrow \text{Fe}^{3+}$
	$N1$	3.30	0.67	0.041/Fe	Related to Fe^{2+} ,
	$P3$	3.90	0.31	0.006/Fe	$\text{CN}^- \rightarrow \text{Fe}^{3+}$
$\text{Co}^{2+\delta}\text{-Fe}^{2+}$	$P1$	2.23	0.64	0.018/Co	$\text{Fe}^{2+} \rightarrow \text{Co}^{3+}$
	$N1$	3.21	0.52	0.027/Co	Related to Co^{2+}
	$P2$	3.80	0.16	0.001/Co	$\text{CN}^- \rightarrow \text{Co}^{3+}$

(*vide infra*). Magnitude of f was estimated from the spectral weight and $\Delta\delta$.

Now, let us proceed to the assignment of the respective components observed in Figs. 3(c) and 3(d). The valence-differential spectroscopy indicates that the positive (negative) components in $\text{Co}^{2+\delta}\text{-Fe}^{2+\delta}$ [Fig. 3(c)] can be assigned to the optical transitions related to the Fe^{3+} (Fe^{2+}) state, while those in $\text{Co}^{2+\delta}\text{-Fe}^{2+}$ [Fig. 3(d)] can be assigned to the transitions related to the Co^{3+} (Co^{2+}) state. The absorption edge of $\text{Co}^{2+\delta}\text{-Fe}^{2+\delta}$ ($\text{Co}^{2+\delta}\text{-Fe}^{2+}$) is ascribed to charge-transfer transition of an electron from the Co^{2+} to Fe^{3+} site (from the Fe^{2+} to Co^{3+} site).⁹ The corresponding positive signals [$P1$ in Figs. 3(c) and 3(d)] are observed in both the films around the absorption edge. In $\text{Co}^{2+\delta}\text{-Fe}^{2+\delta}$ [Fig. 3(c)], the higher-lying positive components ($P2$ and $P3$) can be ascribed to charge-transfer of an electron from the ligand (CN group) to low-spin Fe^{3+} (t_{2g}^5) site. The doublet structure is due to the ligand field splitting ($10Dq$) of the final states, since the observed value ($=1.17$ eV) is comparable with the $10Dq$ for the Fe^{3+} ion.^{10,11} The negative component ($N1$) is related to the low-spin Fe^{2+} (t_{2g}^6) site, and is reasonably ascribed to intramolecular transition within $[\text{Fe}^{2+}(\text{CN})_6]^{4-}$. In $\text{Co}^{2+\delta}\text{-Fe}^{2+}$ [Fig. 3(d)], on the other hand, the higher-lying positive components ($P2$) is due to charge transfer of an electron from the ligand to low-spin Co^{3+} (t_{2g}^6) site. The negative component ($N1$) is related to the high-spin Co^{2+} ($t_{2g}^5 e_g^2$) site. Looking at Table I, one may notice that the transition energy of the $P3$ component in $\text{Co}^{2+\delta}\text{-Fe}^{2+\delta}$ is very close to that of the $P2$ component in $\text{Co}^{2+\delta}\text{-Fe}^{2+}$, suggesting a strong hybridization between the Co^{2+} and Fe^{2+} sites. Such a hybridization perhaps plays a significant role in the thermally and/or photoinduced charge-transfer transition⁹ observed in the Co-Fe cyanides.

The valence-differential spectroscopy has several advantages over conventional spectroscopy. First, the spectroscopy selectively extracts the spectral components related to the oxidized/reduced metal site as positive/negative signals. The resultant sign modulation within the spectra enables accurate and unambiguous spectral decomposition as well as well-founded assignment. Actually, assignments listed in Table I are consistent with the assignments based on the conventional spectroscopy on a series of valence-controlled Co-Fe films.^{7,8} In addition, magnitudes of the optical constants are more reliable in the present investigation, because all the parameters, i.e., E , Γ , and f , can be determined by least-

square fitting of the spectra without any assumptions and/or constraints. Second, the spectroscopy significantly reduces light scattering effect as well as sample/position dependence of the spectra, because the spectra were measured at exactly the same position before and after the electronic pulses. Actually, small signal of the order of 10^{-3} can be discernible in the present experiment. Third, the spectroscopy is widely applicable to the other solid films. In the case of the film whose oxidized/reduced state is unstable, a transient spectroscopy under an external electric pulse is possible. Actually, we applied a transient spectroscopy to $\text{Fe}[\text{Fe}(\text{CN})_6]_{3/4}\cdot 3.5\text{H}_2\text{O}$ film, and obtained reliable differential spectra. In addition to an intense charge-transfer transition at 1.8 eV, we observed a doublet structure at 2.9 and 3.8 eV. The doublet structure can be assigned to charge-transfer of an electron from the ligand to low-spin Fe^{3+} (t_{2g}^5) site. Thus, the valence-differential spectroscopy is a promising tool to clarify complicated electronic structure of solid films, such as Prussian blue analogs and other electrochromic materials.

This work was supported by a Grant-In-Aid for Scientific Research from the Ministry of Education, Culture, Sports, Science and Technology (Grant No. 20045001-A02 0001) and the Support Center for Advanced Telecommunication (SCAT) foundation.

¹A. Gotoh, H. Uchida, M. Ishizaki, T. Satoh, S. Kaga, S. Okamoto, M. Ohta, M. Sakamoto, T. Kawamoto, H. Tanaka, M. Tokumoto, S. Hara, H. Shiozaki, M. Yamada, M. Miyake, and M. Kurihara, *Nanotechnology* **18**, 345609 (2007).

²S. Hara, H. Tanaka, T. Kawamoto, M. Tokumoto, M. Yamada, A. Gotoh, H. Uchida, M. Kurihara, and M. Sakamoto, *Jpn. J. Appl. Phys., Part 2* **46**, L945 (2007).

³F. Herren, P. Fischer, A. Ludi, and W. Halg, *Inorg. Chem.* **19**, 956 (1980).

⁴K. Itaya, I. Uchida, and V. D. Neff, *Acc. Chem. Res.* **19**, 162 (1986).

⁵O. Sato, S. Hayami, Y. Einaga, and Z. Z. Gu, *Bull. Chem. Soc. Jpn.* **76**, 463 (2003).

⁶E. D. L. Dangui, E. Codjovi, H. Tokoro, P. R. Dahoo, S. Ohkoshi, and K. Boukheddaden, *Phys. Rev. B* **78**, 014303 (2008).

⁷F. Nakada, H. Kamioka, Y. Moritomo, J. E. Kim, and M. Takata, *Phys. Rev. B* **77**, 224436 (2008).

⁸K. Igarashi, F. Nakada, and Y. Moritomo, *Phys. Rev. B* **78**, 235106 (2008).

⁹N. Shimamoto, S. Ohkoshi, O. Sato, and K. Hashimoto, *Inorg. Chem.* **41**, 678 (2002).

¹⁰Y. Tanabe and S. Sugano, *J. Phys. Soc. Jpn.* **9**, 766 (1954).

¹¹O. G. Holmes and D. S. McClure, *J. Chem. Soc.* **26**, 1686 (1957).